Comprehensive numerical analysis of a surface-plasmon-resonance sensor based on an H-shaped optical fiber

Mikhail Erdmanis,[1,*] Diana Viegas,[2,3] Markus Hautakorpi,[1] Steffen Novotny,[1] José Luis Santos,[2,3] and Hanne Ludvigsen[1]

[1]*Fiber Optics Group, Department of Micro and Nanosciences, Aalto University, P.O. Box 13500, FI-00076 Aalto, Finland*

[2]*Department of Physics, Faculty of Sciences, University of Porto, Rua de Campo Alegre, 687, 4169-007 Porto, Portugal*

[3]*INESC Porto, Rua Dr. Roberto Frias, 378, 4200-465, Portugal*

**mikhail.erdmanis@aalto.fi*

Abstract: We present and numerically characterize a surface-plasmon-resonance sensor based on an H-shaped optical fiber. In our design, the two U-shaped grooves of the H-fiber are first coated with a thin gold layer and then covered by a uniform titanium dioxide layer to facilitate spectral tuning of the device. A finite element method analysis of the sensor indicates that a refractive-index resolution of up to $5 \cdot 10^3$ nm/RIU can be obtained.

OCIS codes: (060.2280) Fiber design and fabrication; (060.2370) Fiber optics sensors; (240.6680) Surface plasmons.

References and links

1. S. A. Maier, *Plasmonics: Fundamentals and Applications* (Springer, 2007).
2. A. Otto, "Excitation of non-radiative surface plasma waves in silver by the method of frustrated total reflection," Z. Phys. **216**, 398–410 (1968).
3. E. Kretschmann and H. Raether, "Radiative decay of non-radiative surface plasmons excited by light," Z. Naturforsch. **23A**, 2135–2136 (1968).
4. M. Kanso, S. Cuenot, and G. Louarn, "Sensitivity of optical fiber sensor based on surface plasmon resonance: modeling and experiment," Plasmonics **3**, 49–57 (2008).
5. B. D. Gupta and R. K. Verma, "Surface plasmon resonance-based fiber optic sensors: principle, probe designs, and some applications," J. Sensors **2009** (2009).
6. B. Lee, S. Roh, and J. Park, "Current status of micro- and nano-structured optical fiber sensors," Opt. Fiber Technol. **15**, 209–221 (2009).
7. J. M. Fini, "Microstructure fibres for optical sensing in gases and liquids," Meas. Sci. Technol. **15**, 1120-1128 (2004).
8. O. Frazão, J. Santos, F. Araújo, and L. Ferreira, "Optical sensing with photonic crystal fibers," Laser Photon. Rev. **2**, 449-459 (2008).
9. M. Skorobogatiy, "Microstructured and photonic bandgap fibers for applications in the resonant bio- and chemical sensors," J. Sensors **2009**, 524237 (2009).
10. P. St. J. Russell, "Photonic-crystal fibers," J. Lightwave Technol. **24**, 4729–4749 (2006).
11. M. Hautakorpi, M. Mattinen, and H. Ludvigsen, "Surface-plasmon-resonance sensor based on three-hole microstructured optical fiber," Opt. Express **16**, 8427-8432 (2008).
12. A. Csaki, F. Jahn, I. Latka, T. Henkel, D. Malsch, T. Schneider, K. Schröder, K. Schuster, A. Schwuchow, R. Spittel, D. Zopf, and W. Fritzsche, "Nanoparticle layer deposition for plasmonic tuning of microstructured optical fibers," Small **6**, 2584–2589 (2010).
13. F. M. Cox, R. Lwin, M. C. J. Large, and C. M. B. Cordeiro, "Opening up optical fibres," Opt. Express **15**, 11843–11848 (2007).

#146333 - $15.00 USD Received 21 Apr 2011; revised 16 Jun 2011; accepted 17 Jun 2011; published 7 Jul 2011

14. A. Wang, A. Docherty, B. T. Kuhlmey, F. M. Cox, and M. C. J. Large, "Side-hole fiber sensor based on surface plasmon resonance," Opt. Lett. **34**, 3890–3892 (2009).
15. H.-J. Kim, O.-J. Kown, S. B. Lee, and Y.-G. Han, "Measurement of temperature and refractive index based on surface long-period gratings deposited onto a D-shaped photonic crystal fiber," Appl. Phys. B **102**, 81–85 (2011).
16. T. Allsop, R. Neal, C. Mou, P. Brown, S. Rehman, K. Kalli, D. J. Webb, D. Mapps, and I. Bennion, "Multilayered coated infra-red surface plasmon resonance fibre sensors for aqueous chemical sensing," Opt. Fiber Technol. **15**, 477–482 (2009).
17. N. Díaz-Herrera, Ó. Esteban, M.-C. Navarrete, A. González-Cano, E. Benito-Peña, and G. Orellana, "Improved performance of SPR sensors by a chemical etching of tapered optical fibers," Opt. Lasers Eng. **49**, 1065–1068 (2011).
18. Y. Shevchenko, C. Chen, M. A. Dakka, and J. Albert, "Polarization-selective grating excitation of plasmons in cylindrical optical fibers," Opt. Lett. **35**, 637–639 (2010).
19. O. Frazão, T. Martynkien, J. M. Baptista, J. L. Santos, W. Urbanczyk, and J. Wojcik, "Optical refractometer based on a birefringent Bragg grating written in an H-shaped fiber," Opt. Lett. **34**, 76–78 (2009).
20. D. Viegas, M. Hautakorpi, A. Guerreiro, J. L. Santos, and H. Ludvigsen, "Surface-plasmon-resonance sensor based on H-shaped optical fibre," in "Fourth European Workshop on Optical Fibre Sensors," J. M. L.-H. J. L. Santos, B. Culshaw and W. N. MacPherson, eds. (Proc. SPIE, 2010), 7653.
21. M.-C. Navarrete, N. Diaz-Herrera, A. Gonzalez-Cano, and O. Esteban, "A polarization-independent SPR fiber sensor," Plasmonics **5**, 7–12 (2010).
22. H. Aouani, J. Wenger, D. Gérard, H. Rigneault, E. Devaux, T. W. Ebbesen, F. Mahdavi, T. Xu, and S. Blair, "Crucial role of the adhesion layer on the plasmonic fluorescence enhancement," ACS Nano **3**, 2043–2048 (2009).
23. X. Jiao, J. Goeckeritz, S. Blair, and M. Oldham, "Localization of near-field resonances in bowtie antennae: influence of adhesion layers," Plasmonics **4**, 37–50 (2009).
24. E. G. Neumann, *Single-Mode Fibers: Fundamentals* (Springer-Verlag, 1988), p. 88.
25. E. D. Palik, *Handbook of Optical Constants of Solids* (Academic Press, 1998).
26. COMSOL, Inc., Burlington, MA., USA, *COMSOL Multiphysics*. http://www.comsol.com/.
27. D. Monzón-Hernández, J. Villatoro, D. Talavera, and D. Luna-Moreno, "Optical-fiber surface-plasmon resonance sensor with multiple resonance peaks," Appl. Opt. **43**, 1216–1220 (2004).
28. S. Singh, K. Verma, and B. D. Gupta, "Surface plasmon resonance based fiber optic sensor with symmetric and asymmetric metallic coatings: a comparative study," Sens. Transducers J. **100**, 116–124 (2009).

1. Introduction

The resonant formation of surface plasmon waves traveling along the interface between a metallic layer and a dielectric medium has been identified as a phenomenon sensitive to even the smallest changes in the refractive index of the surrounding medium. Optical sensors have successfully utilized this mechanism for accurate measurements of various physical, chemical and biological parameters, finding their way into numerous commercial products in the past decades [1].

Surface plasmon waves, or surface plasmon polaritons (SPP), are excitations on the metal-dielectric interface caused by coupling of an electromagnetic field to the charge-density oscillations on the metal surface. The surface plasmon sensors make use of the extreme sensitivity of this coupling to the material properties at the metal surface. In the most common sensor configurations, the plasmon waves are excited by evanescent fields present at total internal reflection on a prism surface [2,3]. This generally requires bulky components and restricts the use of such devices to laboratory environment. The use of optical fibers instead of the prism has opened the way towards applications of remote sensing based on surface plasmon resonance (SPR), thus offering many advantages such as compact size and low cost. This has drawn a lot of attention and many groups have studied both experimentally and theoretically various optical-fiber-based sensor designs [4–6]. Two parameters are typically used to describe the performance of the sensor: sensitivity and signal-to-noise ratio. It should, however, be stressed that for detailed comparisons, the intended application of the sensor, and e.g., the spectral range and the expected variation of the refractive index, should also be taken into account.

In the past years, the need to analyze ever smaller sample volumes has raised an interest in all-in-fiber sensors that make use of modern microstructured optical fiber (MOF) [7–9]. This type of fiber is typically characterized by a solid or hollow core surrounded by a microstructured

#146333 - $15.00 USD Received 21 Apr 2011; revised 16 Jun 2011; accepted 17 Jun 2011; published 7 Jul 2011

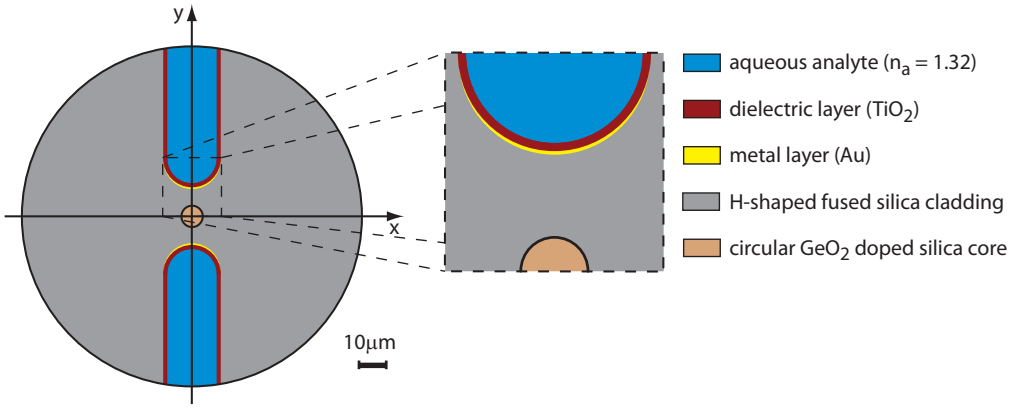

Fig. 1. Cross section of the H-shaped fiber sensor.

cladding which consists of an array of air holes running along the length of the fiber [10]. In closed-form all-in-fiber sensors these micrometer-sized pores are intended to be infiltrated by the analyte [11]. However, despite recent progress, coating the walls of the holes with a thin metal layer still remains a challenge [12]. Furthermore, the response time determined by the filling of the microstructure holes through capillary action and diffusion is typically slow, making online sensing difficult. More feasible are open-structured MOF sensors in which the grooves can easily be coated with metal and where the analyte is in unobstructed contact with the metal surface [13–15]. These combine the sensing advantages of microstructured optical fibers with those of ordinary metal coated optical fibers with, e.g., D-shaped, tapered cross-section or tilted grating [16–18].

In this work, we propose an open-structured SPR fiber sensor design and present a comprehensive numerical characterization based on the finite element method (FEM). The basic fiber geometry follows the structure of an H-shaped optical fiber, similar to the one that has previously been incorporated in an optical refractometer [19]. The potential for SPR sensor operation in the O-band near the 1.3-micron wavelength has recently been explored in a theoretical study [20]. Here, we further develop the fiber geometry for improved sensing performance and highest coupling efficiency to standard a single mode fiber. In particular, this has motivated us to select a circular core with a low doping level for the fiber. Coating the grooves with two layers, a metallic and a uniform high-index dielectric layer, we show that SPPs can resonantly be excited and that they can extend into the openings filled with the analyte. We investigate the influence of the key parameters of the design on the overall performance of the sensor. Our aim is to tailor the device characteristics for aqueous analyte sensing within the C-band, near 1550 nm, taking advantage of the low transmission losses, commercially available light sources, and standard fiber components. We find for this experimentally feasible sensor design a sensitivity, which is to our knowledge among the highest reported for fiber sensors within the specified wavelength and refractive index range, see e.g. [6, 16, 18].

2. Sensor structure and modeling

A schematic drawing of the proposed sensor's fiber cross section is shown in Fig. 1. The basic structure of the sensor forms an H-shaped fiber, produced by chemical etching of an original side-hole silica fiber [19]. The physical dimensions are matched to those of widely used single mode fibers, such as Corning SMF-28, having a circular up-doped core with a diameter of 8.2 μm and a pure silica cladding of 125 μm. This efficiently minimizes the splicing and

#146333 - $15.00 USD Received 21 Apr 2011; revised 16 Jun 2011; accepted 17 Jun 2011; published 7 Jul 2011

coupling losses inherent to many other fiber sensors. The width of the grooves is set to 20 μm, resulting from the optimized trade-off between the mechanical stability of the fiber, good accessibility for metal deposition and a rapid filling with the analyte (refractive index n_a), necessary for real-time remote sensing.

The open structure of the H-shaped fiber particularly facilitates the coating of the inner walls as standard, well established techniques can be used. Here we consider to cover the U-shaped grooves with two layers: a thin metal layer, which supports the SPPs, and a dielectric layer on top, which is required for spectral tuning and protection of the metal layer. We select gold for the metal layer as it is chemically stable and offers exceptional plasmonic properties. Applying the gold layer, for instance, by thermal evaporation [21] we can expect to achieve a non-uniform metal thickness inside the groove with its maximum closest to the core as illustrated in Fig. 1. Onto the complete surface of the U-shaped grooves a uniform dielectric layer of titanium dioxide (TiO_2) is then added, which is most beneficial for spectral tuning thanks to its particularly high refractive index. In order to improve the adhesion of the gold layer to the pure silica grooves we suggest to also add a thin ($\leq$ 5 nm) TiO_2 layer between the bare grooves and the gold coating. Although the adhesion is not as strong as with the typically used Cr or Ti coatings [22], SPP excitation is unlike by these common coatings not suppressed by TiO_2 [23]. In fact, the TiO_2 adhesion layer further contributes to the spectral tuning of the SPR wavelength and is thus treated in the calculations as part of the outer TiO_2 tuning layer to reduce computation time.

Surface plasmon polaritons are excited when the propagation constant along the fiber axis of the core mode and the one of the plasmonic mode match each other. Through the coupling to the plasmonic mode the guided light inside the core becomes highly sensitive to the environment of the fiber, i.e. the refractive index of the analyte. In order to find the coupling condition it is generally necessary to describe the mode propagation inside the core by a complex wavenumber

$$k = \beta - j\frac{1}{2}\alpha, \tag{1}$$

where α is the attenuation constant and β the propagation constant expressed by

$$\alpha = 2k_0 \,\mathrm{Im}\{n_{\mathrm{eff}}\}, \text{and} \tag{2}$$

$$\beta = \mathrm{Re}\{n_{\mathrm{eff}}\}\, k_0. \tag{3}$$

Here, n_{eff} is the effective refractive index of the mode and k_0 the vacuum wavenumber. The decay of the light power P along the fiber axis is then given by

$$P(z) = P_0 \exp(-\alpha z), \tag{4}$$

where z is the propagation distance and P_0 is the initial power at $z = 0$. Once the mode propagation is calculated both for the core and the plasmonic mode, the phase matching condition is identified as requirement of equality between their wavevectors $k_{core} = k_{spp}$. The wavevector of the SPP mode can be approximated by

$$k_{spp} \approx \frac{\omega}{c}\left(\frac{\varepsilon_m \varepsilon_d}{\varepsilon_m + \varepsilon_d}\right)^{1/2} \tag{5}$$

with ω and c describing the angular frequency and the speed of the light, respectively. The parameters ε_m and ε_d are the dielectric constant of the metal and of the surrounding dielectric media. Please note, that in our case ε_d represents an average value determined by the TiO_2 layer, the cladding and the aqueous analyte and can be expressed by a weighted integral of the ε profile over the mode area, analogous to Eq. (5.47) in [24] for standard optical fibers.

#146333 - $15.00 USD Received 21 Apr 2011; revised 16 Jun 2011; accepted 17 Jun 2011; published 7 Jul 2011

From Eq. (5) we find that the resonance wavelength can freely be tuned by adjusting the metal and dielectric coatings, or conversely, the refractive index of the aqueous analyte can be precisely determined for a given layer structure.

Many computational approaches have been used to find the resonant condition for the propagation constant. In most studies the optical fiber is simplified to a one- or two-dimensional layer structure in order to reduce the computation time. Here, we select a full-vectorial FEM analysis to study the light propagation inside the fiber structure. Compared for instance to the transfer matrix formalism, where only a small portion of the fiber is considered and the structure is reduced to a parallel multilayer system [4, 20], the FEM approach allows us to retain the exact cross-sectional structure of the fiber.

First, the refractive indices of the fused silica cladding and the GeO_2 doped silica core are calculated using the Sellmeier equations. The refractive index of the gold layer as a function of wavelength was extracted by linear interpolation from tabulated values [25], whereas for the TiO_2 layer and the aqueous analyte, here represented by water, constant values of 2.65 and 1.32, respectively, were used.

The geometry of the fiber cross section, with reflection symmetry along the *x*-axis, favors one of the light polarization states in contributing to the SPP excitation over the other. Only light guided inside the fiber with an electric field vector lying in the *y*-*z* -plane perpendicular to the metal-dielectric interface can efficiently induce SPP waves. Consequently, we can simplify our 2D computational model without loss of accuracy to one half of the original structure and introduce an artificial boundary condition (perfect electric conductor) along the *x*-axis crossing the core. Moreover, we can speed up the simulation for intermediate results by considering only the geometry inside a 20 μm radius from the fiber center. The highest accuracy results presented here include the complete cladding radius. Furthermore, we smoothly terminated sharp edges of the metal layer in order to avoid any artificial effects caused by local field enhancement.

Taking these parameters and geometrical conditions into account, we modeled the light propagation using a FEM eigenmode solver [26] for perpendicular hybrid-mode waves to determine the wavelength dependent mode profiles and propagation constants.

3. Results

As an example, we show in Fig. 2(a) the calculated effective index values of the core and plasmonic modes as a function of wavelength together with the core mode loss in the vicinity of the SPR. The data are based on optimized sensor parameters, represented by 4 mole% GeO_2 doping of the core, 9 μm distance from the core edge to the groove bottom, 30 nm and 71 nm thicknesses for the gold and dielectric layer, respectively, and considering a constant refractive index $n_a = 1.32$ for the analyte. The maximum of the fiber core mode loss coincides with the avoided crossing of the two effective indices at ≈1540 nm. Two distributions showing the longitudinal power flow through a plane perpendicular to the optical axis are compared in Fig. 2(b): one at off-resonance (position 1 in Fig. 2(a)) and the other at resonance (position 2 in Fig. 2(a)). The sections correspond to the inset in Fig. 1. While the off-resonance mode profile is strongly confined within the core, coupling between the waveguide and plasmonic modes is observed at resonance. In the latter case, SPP waves are induced at the metal-dielectric interface by transfer of energy between the modes, causing a drastic increase of the core mode loss at resonance. For better illustration, we present in Fig. 2(c) the change in the longitudinal flow of power along the dashed line marked in Fig. 2(b).

The propagation constants of both the core and the plasmonic modes are highly sensitive to the sensor properties. Here, we compare the influence of four key parameters on the sensitivity and spectral response of the sensor: thickness of the metal and dielectric layers, core doping level, and distance between the core edge and the groove. We keep three of the parameters

#146333 - $15.00 USD Received 21 Apr 2011; revised 16 Jun 2011; accepted 17 Jun 2011; published 7 Jul 2011

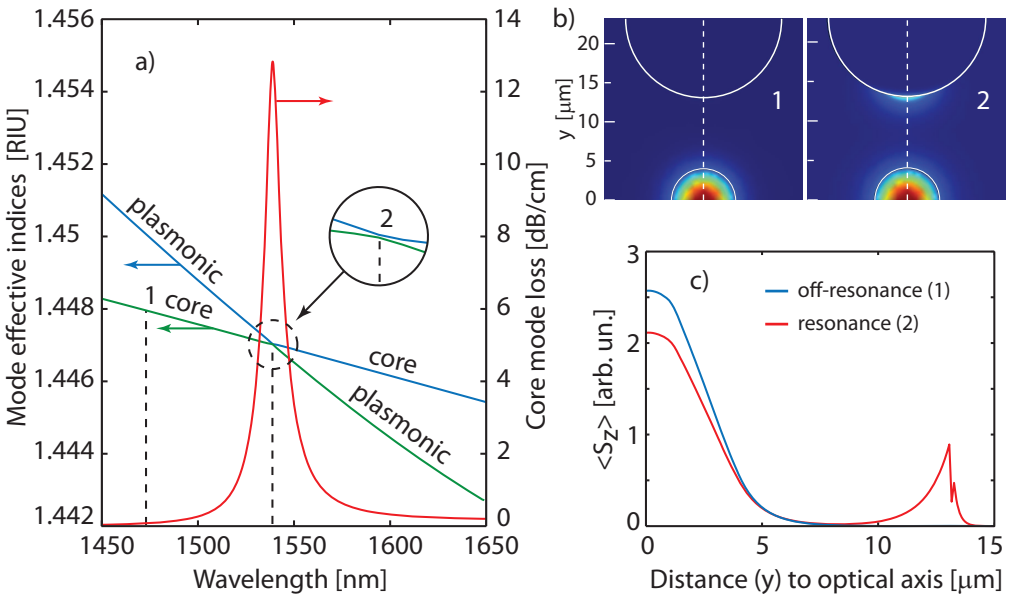

Fig. 2. (a) Real parts of the effective indices of the fundamental core and plasmonic modes (RIU - Refractive index unit) and the fundamental core mode loss (red) as a function of wavelength. (b) Distribution of the longitudinal component of the fundamental mode Poynting vector in the plane perpendicular to the optical axis. (c) Numerical values of the Poynting vector along the dashed line in (b).

fixed while varying the fourth. The resulting fundamental core mode loss curves are shown in Fig. 3, with the sensor design of Fig. 2 represented by the thick (online: red) line.

First, we analyze the influence of the gold layer thickness *m* on the SPP excitation. From the data presented in Fig. 3(a) we find that with an increase in *m* the resonance shifts towards longer wavelengths and the resonance broadens. On the other hand, decreasing the layer thickness is, in practice, limited by the surface roughness of the metal layer, which ultimately determines the maximum achievable sharpness of the resonance peak. Spectral tuning of the resonance is most efficiently realized by varying the TiO_2 layer thickness *d*. As illustrated in Fig. 3(b) the resonance wavelength experiences a similar but more sensitive dependence on *d*, while the resonance width remains nearly constant throughout the selected tuning range. In the next step we investigate the influence of the fiber material and geometry on the sensor performance. High GeO_2 core doping levels significantly shift the resonance position towards smaller wavelength and result in a flattening of the resonance curve (Fig. 3(c)). While the shift of the wavelength can be readily understood from the phase matching condition due to the change of the core refractive index, peak broadening and the reduced losses are explained by the stronger light confinement inside the core, resulting in weaker SPP excitation. Lowering the GeO_2 core doping level even further will reduce the numerical aperture (NA) of the fiber so that mode field matching with a standard single mode fiber will become less efficient. A reduced coupling strength to the plasmonic mode can partly be compensated for by increasing the depth of each groove, as shown in Fig. 3(d). However, deminishing the distance *l* between the core and the groove will also raise the overall loss and decrease the signal-to-noise ratio (SNR). In the opposite case, increasing *l*, the off-resonance loss level can indeed be reduced significantly but the overall signal strength will also become weaker.

For an estimate of the refractive index resolution of the sensor at optimized design param-

#146333 - $15.00 USD Received 21 Apr 2011; revised 16 Jun 2011; accepted 17 Jun 2011; published 7 Jul 2011

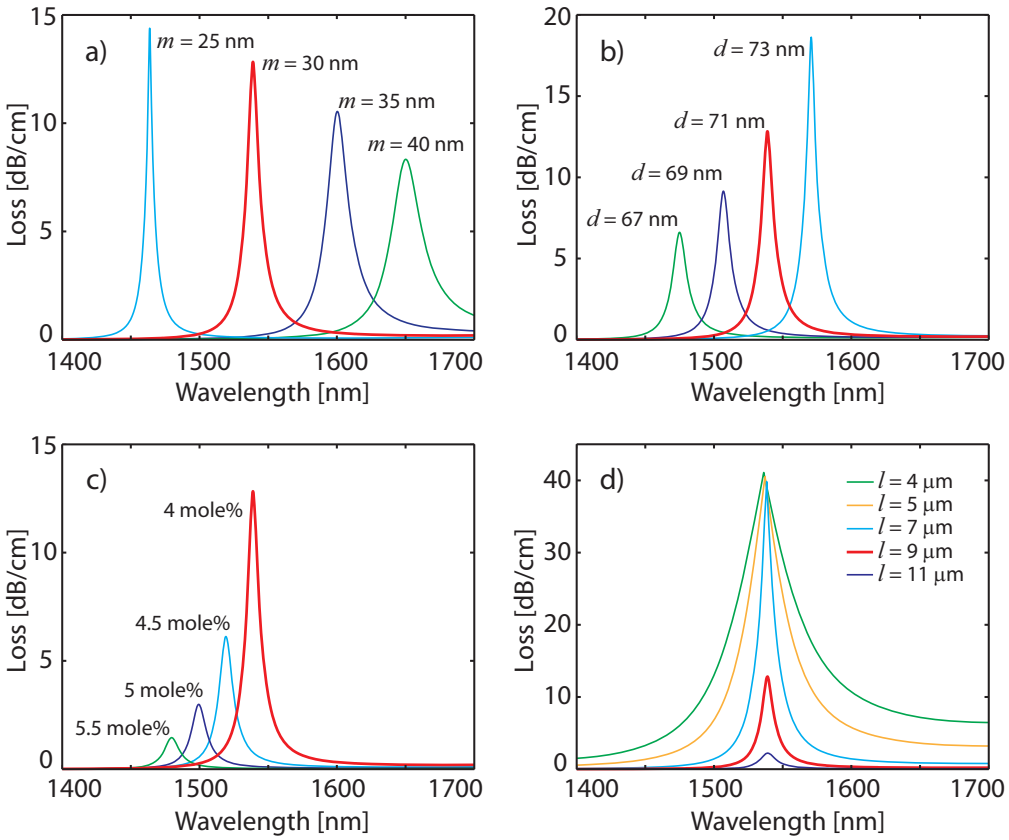

Fig. 3. Fundamental core mode loss spectra for different (a) metal and (b) dielectric layer thicknesses, m and d respectively, (c) core doping levels and (d) distances l between the core edge and the groove bottom.

eters (Fig. 2), we compute the fundamental core mode losses for different analyte refractive indices. Examples of the resulting curves are plotted in Fig. 4(a). From the shift in the resonance wavelength $\Delta\lambda$ induced by a change of the refractive index Δn_a we extract the sensitivity of the fiber sensor as

$$S = \frac{\Delta\lambda}{\Delta n_a} . \tag{6}$$

Considering only aqueous analytes, i.e. $n_a \geq 1.32$, we calculate the sensitivity between different values of n_a with a resonance wavelength either inside (solid circles) or outside (open circle) the specified spectral range of the sensor. We find for the values plotted in Fig. 4(b) a nonlinear response for the sensor. This response of the sensor is in good agreement with experimental measurements of [27, 28], where fiber sensors with asymmetric metal coatings were studied.

Typically, fiber sensors show the highest sensitivity to changes in the surrounding media at low NA, when the difference between the core and cladding indices is small. By varying the core doping level we determine for the fundamental mode the wavelength shift for a change in the analyte refractive index from 1.32 to 1.33. The results, representing the average sensitivity within the selected refractive index range, are presented in Fig. 5. These results show an expected increase in sensitivity at lower values of NA, reaching the highest resolution of up to $5 \cdot 10^3$ nm/RIU at the lowest doping level (4 mole%) considered in the computation. An even

#146333 - $15.00 USD Received 21 Apr 2011; revised 16 Jun 2011; accepted 17 Jun 2011; published 7 Jul 2011

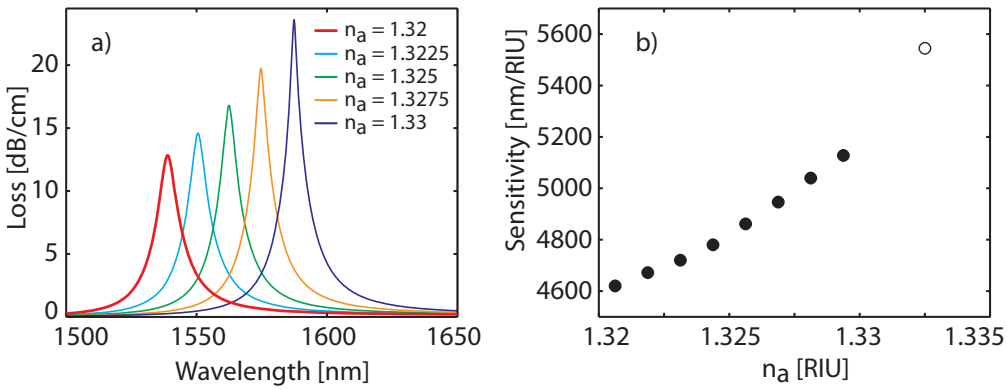

Fig. 4. (a) Fundamental core mode loss spectra and (b) the sensitivity for different analyte refractive indices n_a (solid (open) circle: corresponding resonance wavelength is inside (outside) specified spectral range of the sensor).

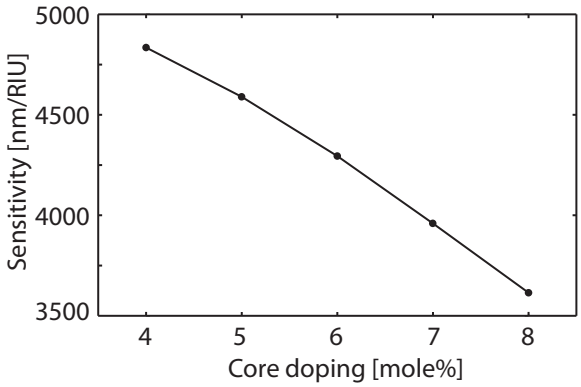

Fig. 5. Estimated average sensitivity for a change of the analyte refractive index by 0.01 from 1.32 to 1.33 calculated for different core doping levels (fundamental core mode).

higher sensitivity can in principle be achieved by further decreasing the core doping level but at the same time this would, as mentioned above, also decrease the coupling efficiency to a standard single mode fiber. Note also that single mode operation is quickly lost when the NA increases and higher order core modes start to participate in the SPP excitation, which happens at core doping levels above ≥ 5 mole%. This will lead to a significant change in the spectral response.

4. Conclusion

We have presented the design and the comprehensive numerical study of an H-shaped optical fiber based SPR sensor for remote real-time sensing of smallest quantities of aqueous analytes. The main design characteristics are the two U-shaped grooves coated by a metal-dielectric double-layer for best analyte sensitivity within the optical C-band together with a circular core to guide the light through the fiber. The analysis has utilized the full-vectorial FEM method in order to take into account the details of the cross-sectional multilayer structure and to identify the key parameters influencing the performance of the sensor.

Considering the actual coating profiles of the grooves, we find the thinnest feasible gold

#146333 - $15.00 USD Received 21 Apr 2011; revised 16 Jun 2011; accepted 17 Jun 2011; published 7 Jul 2011

layer to be the most beneficial to reach a high signal-to-noise ratio, whereas the thickness of the protecting TiO_2 layer on top of the metal layer is chosen to have a value that tunes the sensor operation to the required SPR resonance wavelength range. Off-resonance losses can significantly be suppressed by decreasing the depth of the grooves, but only at the expense of the overall signal amplitude. This leaves only a narrow window between about 7 μm and 9 μm for the optimal choice of the core-groove distance in the fiber design. Another important parameter, the core doping level, has been found to be crucial for two aspects of sensor operation: the signal-to-noise ratio and the sensitivity of the device. We demonstrate numerically that both characteristics are drastically improved for low core doping levels. With single mode operation in the vicinity of 1550 nm and aiming at aqueous analyte sensing, the fiber sensor can achieve the highest sensitivity of up to $5 \cdot 10^3$ nm/RIU for a core doping level of 4 mole%. This is to the best of our knowledge among the highest sensitivities reached by fiber-based aqueous analyte sensing within the C-band.

Particular emphasize was put on the optimization of the fiber design characteristics for the best practical compatibility with standard fiber components. Among those, the fiber's cladding and core sizes were matched to those of the standard single mode fiber, and the circular core with 4 mole% doping level will allow for lossless splicing and efficient coupling. The groove width was selected to provide a high stability of the fiber structure while ensuring at the same time rapid filling of the grooves with the analyte.

We believe that with the presented sensor design we have opened the way towards remote real-time sensing of the smallest liquid analyte samples in a practical and feasible form.

Acknowledgments

This work has been funded by the Academy of Finland (project no. 124165). Part of the work was conducted within the framework of the European COST Actions 299 "Optical Fibres for New Challenges Facing the Information Society" and MP0702 "Towards Functional Sub-wavelength Photonic Structures". D. Viegas acknowledges the Portuguese government for the grant SFRH/BD/30086/2006 in the early stages of this work.

#146333 - $15.00 USD Received 21 Apr 2011; revised 16 Jun 2011; accepted 17 Jun 2011; published 7 Jul 2011